Thermoelectric Magnetohydrodynamic Stirring of Liquid Metals

M. A. Jaworski,* T. K. Gray, M. Antonelli, J. J. Kim, C. Y. Lau, M. B. Lee, M. J. Neumann, W. Xu, and D. N. Ruzic

Center for Plasma-Material Interactions, Department of Nuclear, Plasma, and Radiological Engineering, University of Illinois at Urbana-Champaign, Urbana, Illinois 61801, USA

(Received 10 December 2009; revised manuscript received 25 January 2010; published 5 March 2010)

The direct observation of a thermoelectric magnetohydrodynamic (TEMHD) flow has been achieved and is reported here. The origin of the flow is identified based on a series of qualitative tests and corresponds, quantitatively, with a swirling flow TEMHD model. A theory for determining the dominant driver of a free-surface flow, TEMHD or thermocapillary (TC), is found to be consistent with the experimental results. The use of the analytical form for an open geometry develops a new dimensionless parameter describing the ratio of TEMHD to TC generated flows.

DOI: 10.1103/PhysRevLett.104.094503 PACS numbers: 47.32.Ef, 47.65.−d, 52.30.Cv, 52.55.−s

Current challenges facing the quest for fusion energy have been highlighted in a recent Fusion Energy Sciences Advisory Committee (FESAC) report [1]. Among the top issues facing a power reactor—even present day experiments—is power handling at the plasma-material interface. Current solid materials are subject to large thermal stresses and several programs worldwide are dedicated to testing these materials [1]. An alternative path is that of liquid metal plasma facing components (PFCs) [2].

In the course of testing liquid lithium as a potential PFC [3], the CDX-U experiment made other observations related to its power handling capability [4]. The pool of liquid lithium used in the experiment was subjected to a steady-state electron beam with a peak heat flux of $\approx 60\ \mathrm{MW/m^2}$ without measurable evaporation. Visible and IR imaging of the liquid lithium indicated that flows were produced within the container. The source of this motion was explained as a combination of $\mathbf{J} \times \mathbf{B}$ electron-beam generated forces and a thermocapillary (TC) effect resulting from the temperature dependence of surface tension in liquid lithium [4–6]. The use of such an effect within a strongly magnetized environment (i.e., a divertor) was a natural question following these observations (the electron beam in CDX-U was operated in a range of 200–400 G vs ≥ 1 T in a reactor).

Strong magnetic fields have already been applied in crystal growth experiments to dampen the TC flows generated in crystal melts. Thermoelectric magnetohydrodynamics (TEMHD) was suggested to be operating in these experiments [7] (cf. [8]) but evidence was limited to solidification patterns. TEMHD theory was originally developed by Shercliff with direct application to a fusion environment [9]. The effect is as follows: the thermoelectric effect causes a current to develop between a liquid metal and a container wall when a temperature gradient is present along the interface between them. In the case where there is an external magnetic field which is not parallel to the interface, the Lorentz force results in a net body force on the liquid—a thermoelectric magnetohydrodynamic flow. Use of TEMHD pumping in a porous material is one possible use of the effect in fusion experiments [10].

We report here direct observation of such flows and a dimensionless group describing the relative importance of TEMHD to TC flow effects.

The Solid/Liquid Lithium Divertor Experiment (SLIDE) was used for this study [11,12]. The basics of the experiment consist of an electron beam for producing a line-stripe heat flux, an external magnetic field and target consisting of a pool of liquid lithium held in a stainless steel tray. Figure 1(a) shows a schematic of the experiment. Steady-state operation is achieved with active cooling of the tray and calorimetric measurements are made of the coolant. The target temperature field is measured with two arrays of thermocouples to enable use of a 1D Fourier conduction model to calculate heat flux through the tray. The calculated heat flux is augmented by calorimetric measurements which accounts for 2D effects and losses to the chamber walls. The heat-flux model parameters were determined with an insulated calibration system [12]. Motion of the liquid lithium is monitored visually with a

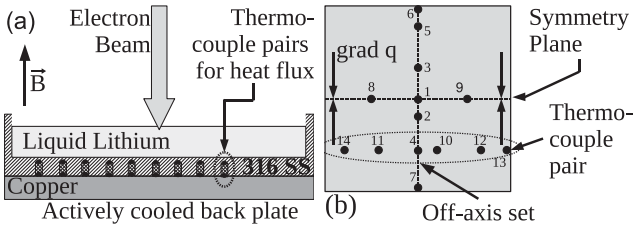

FIG. 1. SLIDE system schematic (a) side view and (b) thermocouple locations (plan view) on right. Thermocouple locations are indicated by the black dots in the figures. For the tests reported in this work, the magnetic field is oriented at normal incidence to the tray as indicated in (a). Visual observation is made from above the system through a vacuum viewport. "Symmetry plane" in (b) corresponds to the location of the line-stripe heat flux and "off axis" refers to the horizontal row of thermocouples parallel to the symmetry plane. Side length of (b) is 10 cm which corresponds to the tray sidewall length. Not to scale.

high-definition digital camera through a viewport. The machine base pressure is 5×10^{-7} Torr.

In these experiments, the electron-beam power was maintained constant at a nominal value of 300 W (15 kV and 20 mA). The electron-beam line stripe was characterized with a Faraday cup at low powers over the range of magnetic fields studied to determine the current density profile for all applied magnetic fields [12]. The magnetic field in these experiments was varied from 34–780 G and the lithium fill was tested at two depths, 5 and 15 mm. The peak heat flux for the highest magnetic field tested was 0.7 MW/m^2 with a heat-flux gradient of 170 MW/(m^2 m).

Figure 2(a) shows the control volume and torques. The torque balance method follows on swirling flow theories [13] and makes use of an approximate linear solution to the Bödewadt-Hartmann flow [14].

Applying angular momentum conservation over the volume V bounded by surface S results in the following [13]:

$$\oint_S (\rho\Gamma)\mathbf{u} \cdot d\mathbf{S} = \int_V (F_\phi r) dV + \oint_S r\tau_\phi \cdot d\mathbf{S}, \quad (1)$$

where $\Gamma = u_\phi r$ is the angular momentum, F_ϕ is the sum of external body forces applied, and τ_ϕ is the shear stress at the wall. Subscript ϕ denotes the azimuthal direction. The external body forces include both TEMHD drive and MHD damping terms. Making use of Karman similarity variables and the approximate linear solution found in [14], the integrals shown in Eq. (1) can be evaluated [12]. The full solution to the torque balance is the following equation:

$$\frac{h\sigma B}{1+C} P\nabla T = \frac{C\sigma B^2}{C+1}\left[\Omega h - (\Omega\nu)^{1/2}\frac{\hat{R}^2(\hat{R}-H_\infty/2)}{1+\hat{R}^2(\hat{R}-H_\infty/2)^2}\right] + \rho\nu^{1/2}\Omega^{3/2}\left[\left(\hat{R}-\frac{H_\infty}{2}\right) + \frac{3\hat{R}^2(\hat{R}-H_\infty/2)}{1+\hat{R}^2(\hat{R}-H_\infty/2)^2}\right], \quad (2)$$

where h is fluid depth, σ is fluid electrical conductivity, B is magnetic induction, P is thermoelectric power of the liquid-solid pair, ∇T is the temperature gradient along the liquid-solid interface, ρ is density, Ω is angular velocity, and ν is kinematic viscosity. $\hat{R}$ is related to a scaling of the boundary layer thickness and H_∞ is related to the vertical outflow from the boundary layer into the core of the rotating flow (see [14] for further details). The parameter, $C = h\sigma/(t\sigma_w)$, where t is the wall thickness and subscript w denotes wall, is the nondimensional ratio of liquid to solid impedances [9]. In order from left to right, the terms of Eq. (2) are as follows: TEMHD drive, MHD braking effects, and the combined viscous and Coriolis terms. Figure 2(b) shows the solution for the angular velocity as a function Hartmann number for a range of values of the C parameter and a constant interface temperature gradient. Flows with magnetic Reynolds number $\mathrm{Re}_M \ll 1$ are assumed in this analysis.

Strong swirling flows were exhibited in all cases where motion of the surface was apparent. A number of qualitative tests were performed to identify the cause of the swirling flow. First, upon reversal of the magnetic field, the flow also reverses. Second, the direction of the swirling flow was found to be consistent with thermoelectric currents as opposed to electron-beam currents as illustrated in Fig. 3. Third, an insulating layer of quartz was introduced between the lithium and the stainless steel and in these cases no motion was generated.

The final test measured the elimination and regeneration of motion after beam shutdown. In this test, a steady swirling motion was generated and the system allowed to come to thermal equilibrium as measured by tray thermocouples. The electron beam was shut down once equilibrium was established. When the magnetic field was also turned off, the fluid was only subject to viscous damping and stopped in 6 s on average. Reapplication of the magnetic field would regenerate motion. When the field was left on, it reacted with any currents remaining in the system and maintained a swirling flow for 190 s on average. The thermal e-folding time constant of the system is calculated to be 78 s based on thermal resistance analysis of the data ($t_{\text{spin down}} \approx 2.4\tau_{\text{thermal}}$).

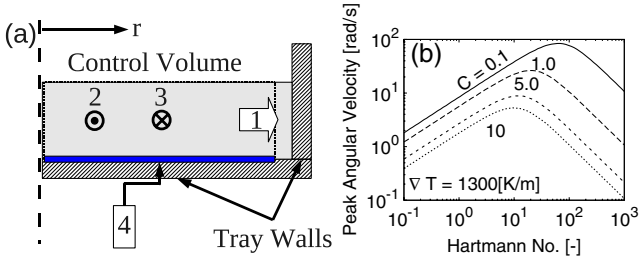

FIG. 2 (color online). Control volume (a) used to calculate the transport of angular momentum within the tray and (b) resulting solution for angular velocity. In (a), numbers denote the following terms: (1) angular momentum transport out of the control volume, (2) TEMHD drive, (3) MHD drag and (4) viscous drag layer. Axis of rotation is indicated on the left. In (b), the solution to the swirling TEMHD, Eq. (2), is shown for several values of C (the dimensionless impedance ratio) for comparison to the duct flow TEMHD analysis reported by Shercliff [9].

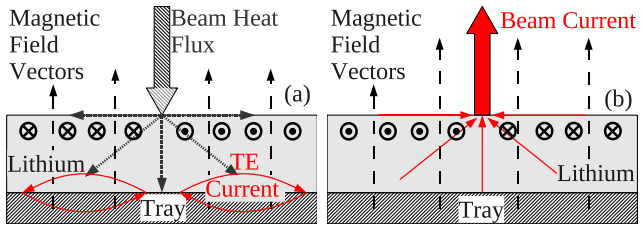

FIG. 3 (color online). Location and direction of the generated thermoelectric currents (a) in response to a local heat flux at the surface of the liquid which radiates outward and (b) electron-beam induced currents. Temperature gradients in (a) responsible for the generation of the TE currents are directed radially inward along the interface between the lithium and tray. Not to scale.

From these qualitative tests it is concluded that TEMHD is the cause of the swirling flow. Tests 1–3 confirm that the swirling flow is consistent with a $\mathbf{J} \times \mathbf{B}$ force directed in a direction consistent with expected TE currents. The inclusion of a resistive layer indicates that the current is operative at the interface of the two materials. The spin-down test demonstrates the independence of the driving currents from the incident electron-beam current. The measured spin-down time with magnetic field is consistent with an effect of thermal origin as is the regeneration of motion after a fast, viscous spin down. The CDX-U and SLIDE tests occur under identical Hartmann numbers and TEMHD is consistent with the observed swirl in CDX-U although not recognized as such at the time of observation [15].

The velocity of the fluid surface is measured by particle tracking. The particles are impurities on the surface of the lithium. The no-slip boundary condition ensures that the fluid velocity at the surface is identical with the observed particles. Laminar flows are expected as the maximum fluid Reynolds number in all cases was below transition ($\mathrm{Re} < 1600$). Significant subsurface gradients in velocity (besides those in the Hartmann layers) are not possible without external current sources as the high Hartmann number of the flow stongly damps viscous effects ($\mathrm{Ha} \geq 18$ for cases with velocity measurements). The experimental setup and steady operation eliminate any such sources resulting in a flow well characterized by the surface velocity.

Temperatures in the tray and the calculated heat fluxes are found to exhibit an axisymmetric profile, as opposed to the linear symmetry of the incident heat flux. The ''off-axis'' set of thermocouples in Fig. 4(c) would indicate uniform heat flux in cases of pure conduction or thermocapillary flows. The Peclet number of liquid lithium flowing at 10 cm/s and a fill depth of 5 mm is $\mathrm{Pe} > 24$ indicating convection dominated thermal transport [10,12]. As the fluid rotates beneath the line-stripe heat flux, the thermal energy is transported with the flow becoming effectively radial as it diffuses into the tray. An axisymmetric heat-flux pattern is therefore indicative of swirling flow even when flow cannot be visually confirmed. The temperature of the interface between the stainless steel and lithium is calculated using the measured temperatures and heat-flux model, Fig. 4 shows an example data set.

Figure 5 shows the results of the comparison of the particle velocity measurements and the predicted velocity from the interface temperature. Temperature dependent material properties are utilized for the theoretical calculations. The model is found to agree within the experimental error to the obtained velocity data. The regression analysis indicates that the ''best fit'' curve is 10% higher for this data set, however this is well within the uncertainty of the set.

The ratio between the computed swirling TEMHD velocity and an expected thermocapillary flow [11,12] in the SLIDE geometry is shown in Fig. 6(a). In all cases where velocity measurements were available, a swirling, TEMHD flow was observed. In all other cases, an axisymmetric heat-flux profile was measured indicating a swirling flow, though of insufficient magnitude to break up the surface impurity layer. Both of these observations are consistent with the predicted dominance of TEMHD flows for these Hartmann numbers.

The same ratio between TC and TEMHD flows can be calculated for a semi-infinite domain. In this case, a closed form solution for the TEMHD flow is available (cf. [9,12]) and elucidates the relevant physical constants. The analyti-

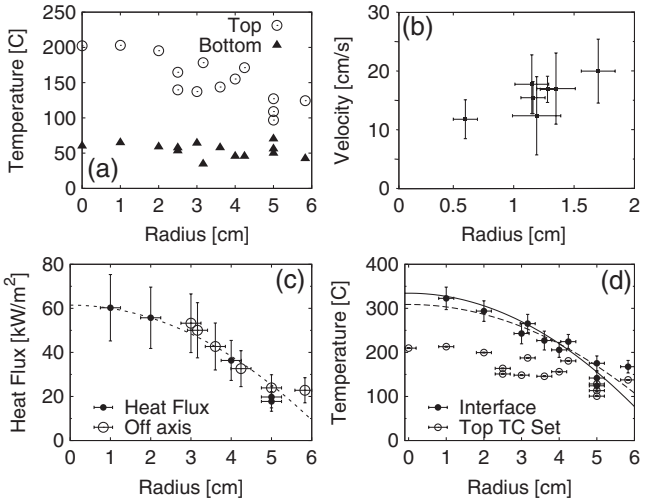

FIG. 4. Example data set showing (a) raw temperature profile, (b) velocity data, (c) heat-flux profile (line drawn to guide the eye) and (d) interface temperature calculation. The parabolic curve fit in (d) is used to calculate the integrated TEMHD drive force of Eq. (2); dashed line corresponds to the 1D model, solid is with the 2D correction. Temperature error bars in (a) are smaller than the size of the data point ($\sigma_T < 0.5\,^\circ\mathrm{C}$).

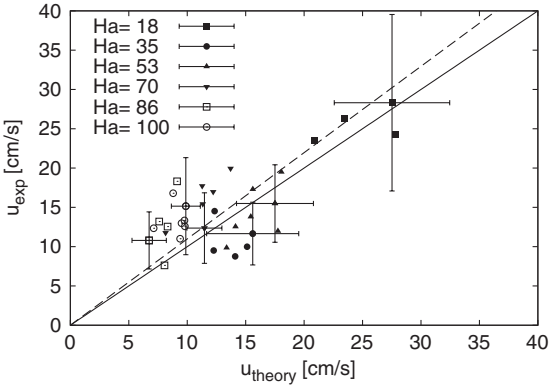

FIG. 5. Comparison of predicted to measured particle velocity. Solid line indicates 1:1 correspondence with prediction of Eq. (2). Dashed line indicates weighted linear least squares ''best fit'' for the data with a slope of 1.1. Typical error bar for each Ha set of data is shown. Reduced χ^2 goodness-of-fit value of the theory curve (best fit) is 0.97 (0.76) indicating a good fit to the data.

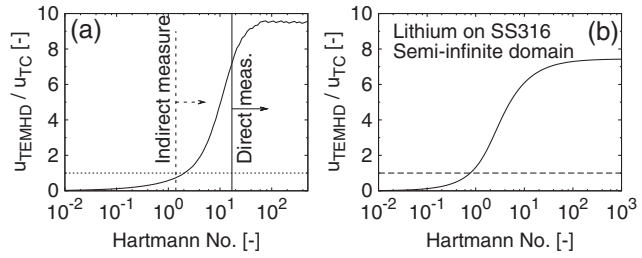

FIG. 6. Predicted ratio of TEMHD to TC flow velocities (a) in the SLIDE geometry and (b) in a semi-infinite domain. ''Direct measurement'' in (a) refers to data sets where velocity data were obtained, ''indirect measurement'' refers to observation of axisymmetric heat-flux profiles indicative of swirling flow, though visual confirmation could not be obtained due to the impurity layer. Calculations in (a) and (b) made for $C = 1$. Oscillations at high values of Ha are due to numerical artifacts.

cal solutions are derived for MHD flows of arbitrary Hartmann number with magnetic Reynolds numbers $\mathrm{Re}_M \ll 1$, which is satisfied in these experiments ($\mathrm{Re}_M \approx 1 \times 10^{-3}$). The resulting form is given as follows and plotted in Fig. 6(b):

$$\frac{u_{\mathrm{TEMHD}}}{u_{\mathrm{TC}}} = \zeta F(\mathrm{Ha}, C), \tag{3}$$

where

$$\zeta = \frac{P(\sigma\rho\nu)^{1/2}}{\gamma} \tag{4}$$

and

$$F(\mathrm{Ha}, C) = \frac{\mathrm{Ha} - \tanh(\mathrm{Ha})}{\mathrm{Ha}\tanh(\mathrm{Ha}) + C\tanh^2(\mathrm{Ha})}, \tag{5}$$

where γ is the surface tension temperature coefficient. The dimensionless quantity ζ is dependent on the container and liquid material properties only and indicates the relative ratio of TEMHD and TC forces. The Hartmann number is denoted by Ha. The function $F(\mathrm{Ha}, C)$ is dependent on the geometry of the flow as well as the dimensionless impedance ratio of the container and fluid C. This formulation assumes the same temperature gradient exists at the free surface and at the liquid-solid interface which is reasonable for thin, conduction dominated fluids. For values of the velocity ratio >1, the flow is expected to be TEMHD dominated. For values of the ratio <1, then the flow is governed by TC effects.

The significance of the TEMHD effect allows for considerable exploitation. While Shercliff's original motivation was self-stirring in large ducts of a fusion blanket [9], porous materials may also be exploited for pumping of the first wall and divertor in a fusion reactor [10] or in the breeder blanket as well. Additionally, this effect may be used in metallurgical applications as a stirring mechanism in addition to, or instead of, rotating magnetic fields [13].

The direct observation of TEMHD driven flows is demonstrated through a series of qualitative experiments. The quantitative scaling agrees with a swirling flow theory based on TEMHD drive forces. The ratio of TEMHD to TC velocities is calculated and indicates regions of TEMHD dominance consistent with the observations of the experiment. A closed form solution for the same ratio yields a dimensionless group depending on material properties of the solid and liquid and the geometry of the flow.

The authors wish to thank R. Kaita, R. Majeski, N. B. Morley, and A. Rockett for input and many useful conversations regarding this work. The reviewer's comments have also been helpful in clarifying the manuscript. This work was supported under DOE Contract No. DEFG02-99ER54515.

*mjaworsk@illinois.edu
http://cpmi.illinois.edu

[1] M. Greenwald *et al.*, Fusion Energy Sciences Advisory Committee technical report, 2006.
[2] M. A. Abdou *et al.* (APEX Team), Fusion Eng. Des. **54**, 181 (2001).
[3] R. Majeski *et al.*, Phys. Rev. Lett. **97**, 075002 (2006).
[4] R. Kaita *et al.*, Phys. Plasmas **14**, 056111 (2007).
[5] J. R. Pearson, J. Fluid Mech. **4**, 489 (1958).
[6] V. G. Levich and V. S. Krylov, Annu. Rev. Fluid Mech. **1**, 293 (1969).
[7] A. Cröll *et al.*, J. Cryst. Growth **183**, 554 (1998).
[8] R. Moreau *et al.*, Mater. Sci. Eng. A **173**, 93 (1993).
[9] J. A. Shercliff, J. Fluid Mech. **91**, 231 (1979).
[10] M. A. Jaworski, N. B. Morley, and D. N. Ruzic, J. Nucl. Mater. **390–391**, 1055 (2009).
[11] M. A. Jaworski and D. N. Ruzic, in *Proceedings of the 22nd IEEE/NPSS Symposium: Fusion Engineering* (IEEE, Albuquerque, NM, 2007).
[12] M. A. Jaworski, Ph.D. thesis, University of Illinois, Urbana, IL, 2009.
[13] P. A. Davidson, J. Fluid Mech. **245**, 669 (1992).
[14] P. A. Davidson and A. Pothérat, Eur. J. Mech. B, Fluids **21**, 545 (2002).
[15] R. Majeski (personal communication).